Journal of Solid State Chemistry 181 (2008) 3071–3077

Contents lists available at ScienceDirect

Journal of Solid State Chemistry

journal homepage: www.elsevier.com/locate/jssc

The first di-cadmium-substituted vanadoarsenate derived from α-{$As_8V_{14}O_{42}$} shell

Dan Zhao [a,b], Shou-Tian Zheng [a], Guo-Yu Yang [a,*]

[a] State Key Laboratory of Structural Chemistry, Fujian Institute of Research on the Structure of Matter, Chinese Academy of Sciences, Fuzhou, Fujian 350002, China
[b] Biology and Chemistry Engineering Department of Fuqing Branch of Fujian Normal University, Fuqing, Fujian 350300, China

ARTICLE INFO

Article history:
Received 6 May 2008
Received in revised form
4 July 2008
Accepted 9 July 2008
Available online 6 August 2008

Keywords:
Polyoxometalate
Vanadoarsenate
Cadmium
Substitute
Hydrothermal synthesis

ABSTRACT

Two di-cadmium-substituted vanadoarsenates, $[Cd(enMe)_3]_2\{\alpha\text{-}[(enMe)_2Cd_2As_8V_{12}O_{40}(0.5H_2O)]\}\cdot 5.5H_2O$ (**1**, enMe = 1,2-diaminopropane) and $[Cd(enMe)_2]_2\{\beta\text{-}[(enMe)_2Cd_2As_8V_{12}O_{40}(0.5H_2O)]\}$ (**2**), were hydrothermally synthesized and characterized by elemental analyses, IR, TGA, UV–Vis, XRD, magnetic measurements and single crystal structural analyses. Crystal data for **1**: monoclinic, $P2(1)/c$, $a = 15.040(9)$ Å, $b = 20.288(12)$ Å, $c = 27.873(17)$ Å, $\beta = 98.046(8)^\circ$, $V = 8421.3(19)$ Å^3, $Z = 4$; for **2**: monoclinic, $P2(1)/n$, $a = 12.753(3)$ Å, $b = 19.334(5)$ Å, $c = 14.310(3)$ Å, $\beta = 99.984(3)^\circ$, $V = 3475.1(14)$ Å^3, $Z = 2$. X-ray diffraction analyses reveal that compounds **1** and **2** exhibit isolated and one-dimensional inorganic–organic hybrid structures, respectively. The former is the first di-cadmium-substituted vanadoarsenate derived from α-{$As_8V_{14}O_{42}$} shell, while the latter is another kind of di-cadmium-substituted vanadoarsenate derived from β-{$As_8V_{14}O_{42}$} shell. Variable temperature susceptibility measurements demonstrate the presence of antiferromagnetic interactions between V^{IV} cations in **1** and **2**.

1. Introduction

Transition-metal-substituted polyoxometalates (TMSPs) exhibit a fascinating variety of structures and properties including catalysis, medicine and magnetism [1]. Within the class of TMSPs, TM-substituted polyoxotungstates (POTs) represent the largest subclass [2]. The preparation of TM-substituted POTs is usually based on various lacunary polyoxoanions such as mono-lacunary $[PW_{11}O_{39}]^{7-}$, dilacunary $[SiW_{10}O_{36}]^{8-}$, trilacunary $[XW_9O_{33}]^{9-}$, multi-lacunary $[P_2W_{12}O_{48}]^{14-}$ and so forth. These lacunary precursors have well-defined metal–cation binding sites and are useful synthons for making novel TM-substituted POTs. Compared with abundant TM-substituted POTs, TM-substituted polyoxovanadates (POVs) are rare because it is hard to obtain steady lacunary POV precursors. So, the design and synthesis of TM-substituted POVs remains challenges for synthetic chemists.

During the past 5 years, we have devoted great efforts to explore reasonable approach for preparing TM-substituted POVs. In 2004, we firstly observed that zinc ions can substitute two VO_5 pyramids of arsenic–vanadium cluster to form di-Zn-substituted POVs [3]. This result offers a feasible approach for making novel TM-substituted POVs. From then on, about nine new TM-substituted POVs were continuously synthesized and reported by us and others [4], including 0D mono-Cd-substituted, dimeric mono/di-Zn-substituted, 1D mono/di-Ni/Zn/Cd-substituted and 2D di-Zn-substituted POVs. These compounds exhibit unique inorganic–organic hybrid structures containing inorganic POV backbones decorated or bridged directly by organic functional groups. As part of continuing work in this system, here we reported the hydrothermal synthesis and structural characterization of the first di-Cd-substituted POV based on α-{$As_8V_{14}O_{42}$} cluster, $[Cd(enMe)_3]_2\{\alpha\text{-}[(enMe)_2Cd_2As_8V_{12}O_{40}(0.5H_2O)]\}\cdot 5.5H_2O$ (**1**, enMe = 1,2-diaminopropane). Interestingly, an increase in the initial quantity of enMe resulted in the crystallization of a 1D di-Cd-substituted POV based on β-{$As_8V_{14}O_{42}$} cluster, $[Cd(enMe)_2]_2\{\beta\text{-}[(enMe)_2Cd_2As_8V_{12}O_{40}(0.5H_2O)]\}$ (**2**).

2. Experimental section

2.1. General methods

All chemicals purchased were of reagent grade and used without further purification. Elemental analyses were determined on a Vario EL III elemental analyzer. IR spectra (KBr pellets) were recorded on an ABB Bomen MB 102 spectrometer. Thermal analyses were performed in a dynamic air atmosphere with a heating rate of 10 °C/min, using a METTLER TGA/SDTA851[e]

* Corresponding author. Fax: +86 591/8371 0051.
E-mail addresses: ygy@fjirsm.ac.cn, guoyu.yang@hotmail.com (G.-Y. Yang).

0022-4596/$ - see front matter © 2008 Elsevier Inc. All rights reserved.
doi:10.1016/j.jssc.2008.07.034

thermal analyzer. Reactions were carried out in 40 ml Teflon-lined steel autoclave at autogenous pressure. The UV–Vis spectra were recorded at room temperature on a PE Lambda 900 UV–Vis spectrometer equipped with an integrating sphere in the wavelength range 200–800 nm. $BaSO_4$ plate was used as a reference (100% reflectance), on which the finely ground powder of the samples were coated. The absorption spectra were calculated from reflection spectra by the Kubelka–Munk function [5]: $\alpha/S = (1-R)^2/2R$, where α is the absorption coefficient, S is the scattering coefficient and R is the reflectance. XRD spectra were obtained using a Philips X'Pert-MPD diffractometer with Cu$K\alpha$ radiation ($\lambda = 1.54056$ Å). Variable temperature susceptibility measurements were carried out in the temperature range 2–300 K at a magnetic field of 1 T on polycrystalline samples with a SQUID MPMS-7 magnetometer manufactured by Quantum Design. Background corrections for the sample holder assembly and diamagnetic components of the compound were applied.

2.2. Synthesis

2.2.1. Synthesis of **1**

A sample of V_2O_5 (0.30 g, 1.65 mmol) and As_2O_3 (0.35 g, 1.77 mmol) was stirred in 10 ml distilled water for 10 min, forming an orange mixed solution. And then a 1.20 ml enMe was added drop by drop with continuous stirring. As a result, the colour of solution shift from orange to yellow-green. Further, to this solution 1.20 g (7.21 mmol) $Cd(OAC)_2 \cdot 2H_2O$ was added and stirred for 30 min. The resulting solution was sealed in a 35 ml stainless steel reactor with a Teflon liner and heated at 170 °C for 3 days, and then cooled to room temperature. The product was isolated as brown blocks (42.3% yield based on V). Anal. Calcd. for ($C_{24}H_{92}As_8Cd_4N_{16}O_{46}V_{12}$): C, 9.60; H, 3.09; N, 7.46 wt%. Found: C, 9.38; H, 3.35; N, 7.32 wt%. IR (KBr, cm^{-1}) for **1**: 3436s, 3328s, 2933w, 2880w, 1587s, 1452w, 1389w, 1353w, 1327w, 976s, 734s, 690s, 573m, 438s.

2.2.2. Synthesis of **2**

Compound **2** was isolated in conditions similar to **1** except an increase in the initial quantity of enMe from 1.20 to 1.60 ml. The product was isolated as brown blocks (31.5% yield based on V). Anal. Calcd. for ($C_{18}H_{61}As_8Cd_4N_{12}O_{40.5}V_{12}$): C, 7.84; H, 2.23; N, 6.10 wt%. Found: C, 7.77; H, 2.38; N, 5.95 wt%. IR (KBr pellet ν/cm^{-1}) for **2**: 3463s, 3310s, 2969w, 2925w, 2862w, 1587s, 1452m, 1389m, 1183w, 976s, 896m, 734s, 690s, 573m, 429s.

2.3. X-ray crystallography

X-ray data were collected at room temperature on a Rigaku Mercury CCD/AFC diffractometer with Mo$K\alpha$ radiation ($\lambda = 0.71073$ Å). Lorentz and polarization corrections as well as empirical absorption correction were carried out for the net intensities [6]. The structures were solved by direct methods and refined by full-matrix least-squares techniques using SHELXTL97 [7]. All non-hydrogen atoms were treated anisotropically in the two complexes. No attempt was made to locate the hydrogen atoms of water. The crystallographic data are summarized in Table 1. Ranges of selected bond distances of **1**–**2** are listed in Table 2. CCDC 686075 and 686076 contain the supplementary crystallographic data for **1** and **2**, respectively. These data can be obtained free of charge via www.ccdc.cam.ac.uk/conts/retrieving.html [or from the Cambridge Crystallographic Data Centre, 12, Union Road, Cambridge CB2 1EZ, UK; fax: (internat.) +44-1223/336-033; or deposit@ccdc.cam.ac.uk].

Table 1
Crystallographic data for compounds **1**–**2**

Compound	**1**	**2**
Formula	$C_{24}H_{92}As_8Cd_4N_{16}O_{46}V_{12}$	$C_{18}H_{61}As_8Cd_4N_{12}O_{40.50}V_{12}$
M_r	3001.38	2754.03
Crystal system	Monoclinic	Monoclinic
Space group	$P2_1/c$	$P2_1/n$
Crystal size (mm)	$0.40 \times 0.30 \times 0.25$	$0.75 \times 0.40 \times 0.12$
a (Å)	15.040(9)	12.753(3)
b (Å)	20.288(12)	19.334(5)
c (Å)	27.873(17)	14.310(3)
β (deg)	98.046(8)	99.984(3)
V (Å^3)	8421.3(19)	3475.1(14))
Z	4	2
D_c (g cm^{-3})	2.367	2.632
μ (mm^{-1})	5.464	6.600
Reflections collected	56491	26326
Unique data (R_{int})	17619 (0.0799)	7938 (0.0556)
$F(000)$	5792	2618
Θ range (deg)	3.10–27.49	3.24–27.48
Goodness of fit	1.136	1.035
R_1, wR_2 [$I > 2\sigma(I)$][a]	0.0987, 0.2178	0.0513, 0.1475
$\Delta\rho_{max}$, $\Delta\rho_{min}$ (e Å^{-3})	1.312, −1.037	2.012, −1.566

[a] $R_1 = \sum||F_o|-|F_c||/\sum|F_o|$; $wR_2 = \{\sum[w(F_o^2-F_c^2)^2]/\sum[w(F_o^2)^2]\}^{1/2}$.

Table 2
Ranges of some important bond lengths (Å) and angles (deg) for compounds **1** and **2**

		1	
V = O	1.600(9)–1.633(10)	Cd–N	2.284(13)–2.427(15)
V–O	1.904(8)–2.011(9)	Cd–O	2.230(9)–2.345(10)
As–O	1.735(9)–1.820(10)	V–V	2.872(4)–3.015(4)
O–V–O	78.6(4)–148.3(4)	O–Cd–O	66.1(3)–123.6(4)
O–As–O	97.0(4)–101.5(4)	O–Cd–N	85.3(4)–152.0(5)
N–Cd–N	70.1(8)–161.8(7)		
		2	
V = O	1.598(4)–1.652(4)	Cd–N	2.241(7)–2.410(4)
V–O	1.929(4)–2.007(4)	Cd–O	2.280(5)–2.535(5)
As–O	1.737(5)–1.803(5)	V–V	2.902(2)–3.107(1)
O–V–O	76.1(2)–147.3(2)	O–Cd–O	67.2(2)–125.6(2)
O–As–O	98.0(2)–101.0(2)	O–Cd–N	72.4(2)–146.6(2)
N–Cd–N	73.7(9)–155.0(3)		

3. Result and discussion

The α-{$As_8V_{14}O_{42}$} shell was first presented by Jacobson et al. in 1991 [8], and its isomer, that is the β-{$As_8V_{14}O_{42}$} shell, was first presented by us in 2005 [9]. Here, we briefly describe the structures of them. As shown in Fig. 1a, the α-{$As_8V_{14}O_{42}$} shell consists of 14 condensed VO_5 square pyramids and eight trigonal pyramids (AsO_3). Among them, eight VO_5 square pyramids share their edges of the base to form a V_8O_{24} ring, while the other six VO_5 square pyramids share their edges to form two arched V_3O_{11} trimers. Then, the V_8O_{24} ring is sandwiched by the two arched V_3O_{11} trimers in a mutually perpendicular mode, resulting in the formation of a {$V_{14}O_{42}$} shell with S_4 symmetry. On the other hand, the eight AsO_3 trigonal pyramids are linked in pairs, through an oxygen bridge, forming four handle-like As_2O_5 units. Finally, four windows of the cage are each capped by a As_2O_5 moiety to give a spherical α-{$As_8V_{14}O_{42}$} shell. The β-{$As_8V_{14}O_{42}$} shell with D_{4h} symmetry can be derived from α-{$As_8V_{14}O_{42}$} shell by a 90° rotation of one-half of the α-{$As_8V_{14}O_{42}$} shell around its S_4 axes (Fig. 1b).

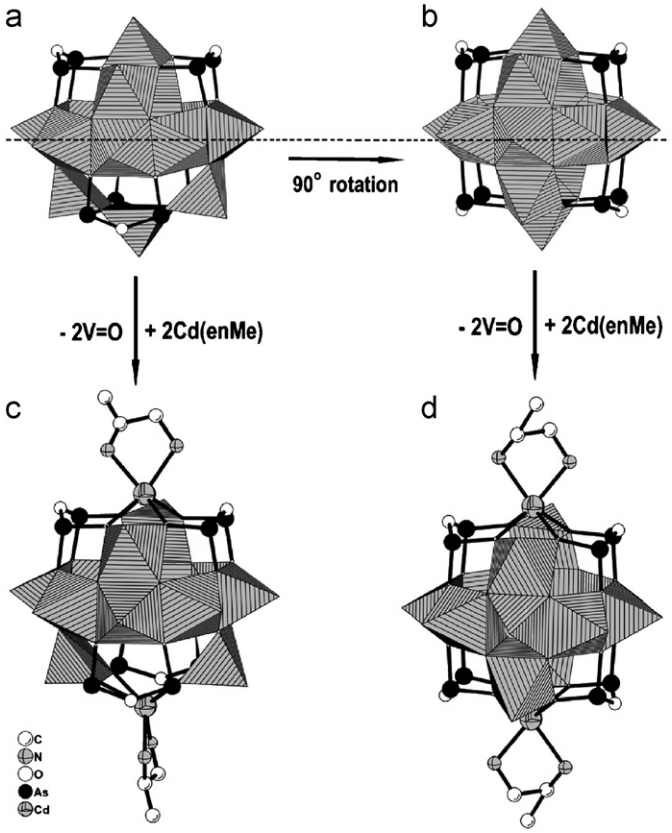

Fig. 1. (a)–(d) View of the structures of α-{$As_8V_{14}O_{42}$}, β-{$As_8V_{14}O_{42}$}, α-{$(enMe)_2Cd_2As_8V_{12}O_{40}$} and β-{$(enMe)_2Cd_2As_8V_{12}O_{40}$} shells, respectively.

Single crystal X-ray diffraction analysis shows that the molecular structure of **1** consists of one inorganic–organic hybrid di-Cd-substituted α-$[(enMe)_2Cd_2As_8V_{12}O_{40}(0.5H_2O)]^{4-}$ polyoxoanion with two isolated $[Cd(enMe)_3]^{2+}$ complexes acting as charge compensation. The structure of new α-$[(enMe)_2Cd_2As_8V_{12}O_{40}(0.5H_2O)]^{4-}$ polyoxoanion can be derived from α-{$As_8V_{14}O_{42}$} shell by replacing the two $[V=O]^{2+}$ units located between As_2O_5 groups with two divalent cadmium complexes $[Cd(enMe)]^{2+}$ (Fig. 1c). Each embedded Cd^{2+} center is coordinated with four O atoms derived from the polyoxoanion and two N atoms from enMe ligand, exhibiting a common hexa-coordination environment but with rare trigonal-prismatic geometry (Fig. 2a). The Cd–O distances vary from 2.230(9) to 2.345(10) Å, which are in good agreement with those found in Cd-containing polyoxometalates [10] but obviously longer than the V–O distances 1.912(8)–2.003(8) Å in **1**. Each isolated Cd^{2+} center is defined by six N atoms from three enMe ligands and display a usual octahedron with the Cd–N distances in the range of 2.284(13)–2.427(15) Å (Fig. 2b).

The 3D packing diagram of **1** can be seen in Fig. 3, the di-Cd-substituted POVs and the isolated $[Cd(enMe)_3]^{2+}$ complexes are aligned parallel to the *ab*-plane to form polyoxoanion layer and cation layer, respectively, which are alternatively stacked along the *c*-axis to form 3D packing structure **1**. Up to now, only two Cd-substituted POVs have been reported, one is 0D mono-Cd-substituted POV $[\alpha\text{-}(dien)CdAs_8V_{13}O_{41}(H_2O)]^{4-}$ and the other is 1D di-Cd-substituted POV $[\beta\text{-}(en)_2Cd_2As_8V_{12}O_{40}]^{4-}$ [4b]. Now, compound **1** exhibits the first di-Cd-substituted POV derived from α-{$As_8V_{14}O_{42}$} shell.

Further, by reducing the quantity of enMe ligand, we attempted to change the isolated cations $[Cd(enMe)_3]^{2+}$ in **1** into $[Cd(enMe)_2]^{2+}$ groups which may act as bridges and link

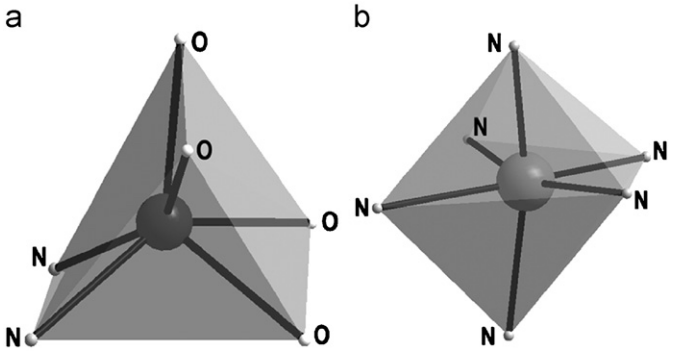

Fig. 2. (a) and (b) View of geometries around the embedded and isolated Cd atoms in **1**, respectively.

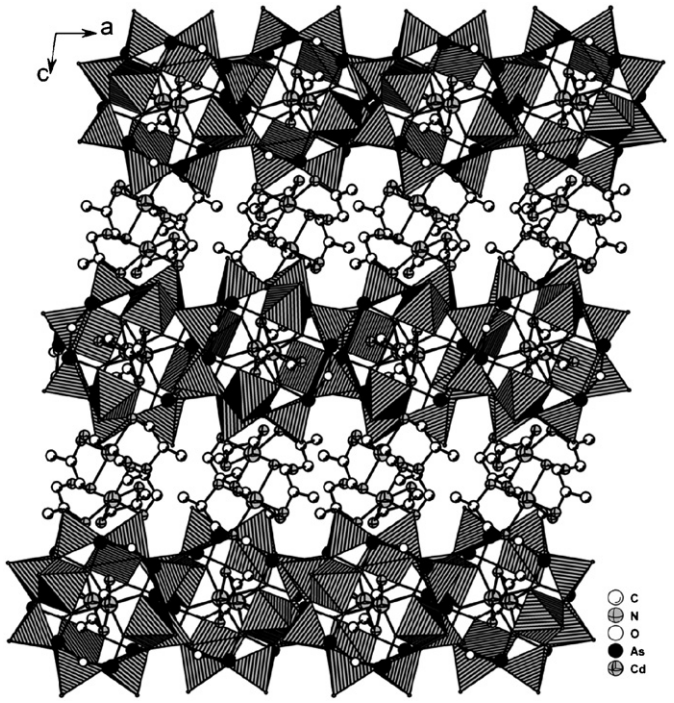

Fig. 3. View of 3D packing diagram of **1** along *b*-axis.

polyoxoanions α-$[(enMe)_2Cd_2As_8V_{12}O_{40}(0.5H_2O)]^{4-}$ to form extended inorganic–organic hybrid framework. Unfortunately, our experiments were unsuccessful. Interestingly, on the contrary, an increase of the quantity of enMe ligand made us obtain compound **2** that possesses 1D infinite structure but constructed from polyoxoanions β-$[(enMe)_2Cd_2As_8V_{12}O_{40}(0.5H_2O)]^{4-}$. Compound **2** is isomorphic with the above-mentioned compound $[Cd(en)_2]_2[(en)_2Cd_2As_8V_{12}O_{40}]$ [4b], except that the en ligands are replaced by enMe ligands. As shown in Fig. 1d, the β-$[(enMe)_2Cd_2As_8V_{12}O_{40}(0.5H_2O)]^{4-}$ can be derived from β-{$As_8V_{14}O_{42}$} shell by replacing a pair of four $[V=O]^{2+}$ units located between As_2O_5 groups with two $[Cd(enMe)]^{2+}$ complexes. In **2**, the polyoxoanions are connected with each other by dual μ_2-$[Cd(enMe)_2]^{2+}$ bridges via V = O–Cd bonds with O–Cd–O angle of 102.3(2)° and Cd–O distances of 2.402(4) and 2.535(5) Å to form infinite linear chains which are aligned parallel to the *c*-axis (Fig. 4). The infinite chains are parallel stacked along *a*-axis to generate chain layers that are parallel to the *ac*-plane (Fig. 5), and then these chain layers are further stacked along the *b*-axis in ABAB sequence to form **2**.

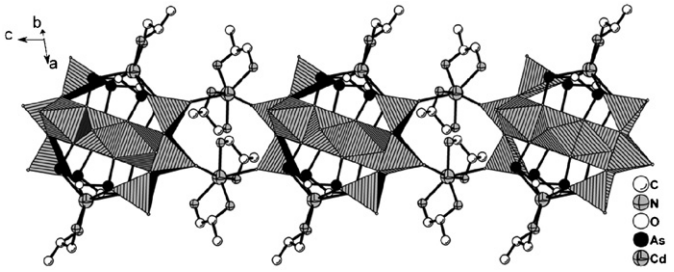

Fig. 4. View of 1D structure of **2**.

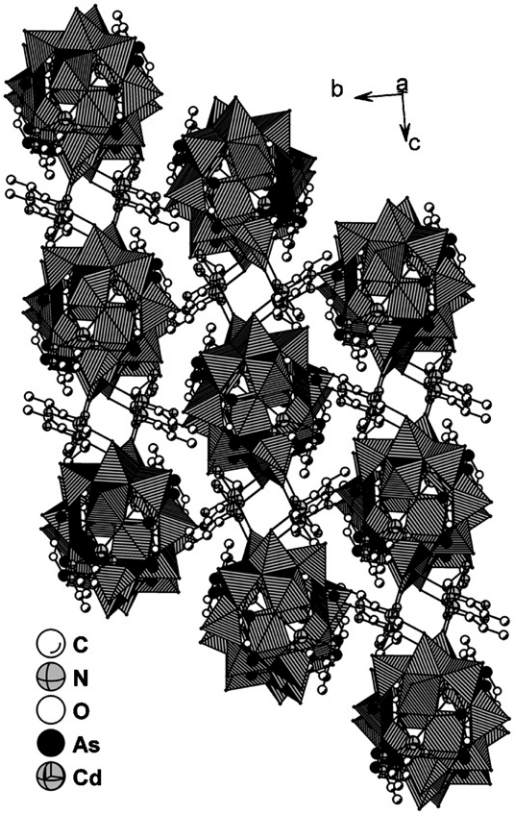

Fig. 5. View of 3D packing diagram of **2** along *a*-axis.

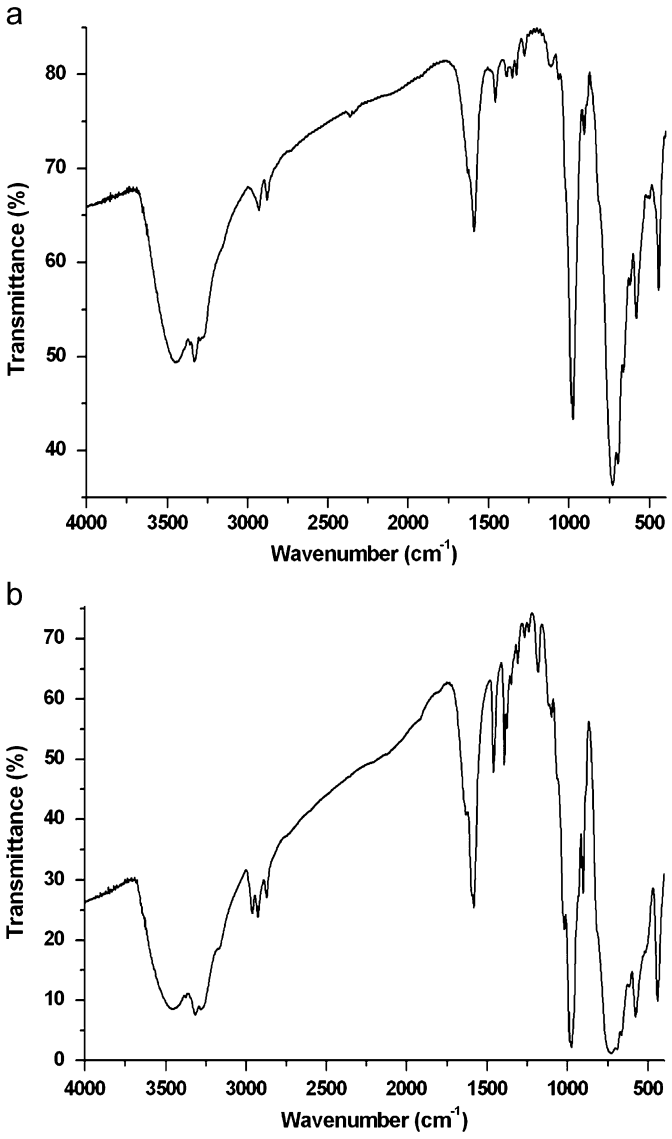

Fig. 6. IR spectra of **1** and **2**.

In **1**–**2**, all V = O, V–O, Cd–O, Cd–N and As–O bond lengths fall in the ranges 1.598(4)–1.652(4), 1.904(8)–2.011(9), 2.230(9)–2.535(5), 2.241(7)–2.427(15) and 1.735(9)–1.820(10) Å, respectively. On the basis of bond valence sum (Σ_s) calculations [11], the oxidation states of all V atoms are +4 ($\Sigma_s = 4.25$–4.39, **1**; $\Sigma_s = 4.28$–4.35, **2**), the Cd atoms are +2 ($\Sigma_s = 1.95$–2.14, **1**; $\Sigma_s = 2.05$–2.10, **2**) and the As atoms are +3 ($\Sigma_s = 3.11$–3.26, **1**; $\Sigma_s = 3.14$–3.16, **2**). The oxidation states of the V, Cd and As atoms are consistent with the overall charge balance of formulas 1 and 2. It is noteworthy that during the course of these two reactions, enMe acts as a reducing agent, which is responsible for the reductions of V^{5+} to V^{4+} and As^{5+} to As^{3+} [3,4].

As shown in Fig. 6, the infrared spectrum of **1** exhibited features characteristic of *v* (*M*–O–*M*) (*M* = V or As) in the 480–800 cm^{-1} region. While the strong peak at 976 cm^{-1} is attributed to the vibrations of V = O bands. The bending bands of the NH_2 and CH_2 present at around 1587, 1452, 1389, and 1327 cm^{-1}. For **2**, the strong band at 976 cm^{-1} ascribed to *v* (V = O) and a series of bands in the 500–805 cm^{-1} region are characteristic of *v* (*M*–O–*M*) (*M* = V or As). The region in determining the mode of enMe binding is from 1168 to 1631 cm^{-1}. As shown in Fig. 7, both TG curves of **1** and **2** show a series of continuous weight losses in the ranges 40–454 °C for **1** and 55–485 °C for **2**, which are attributed to the losses of H_2O, enMe molecules and the sublimation of part As_2O_3 molecules. Further, weight gains occurring from 454 to 555 °C for **1** and from 485 to 625 °C for **2** were consistent with the oxidation of V atoms form V^{4+} to V^{5+} and part As atoms from As^{3+} to As^{5+}. As shown in Figs. 8 and 9, XRD powder diffractions indicate that the structure of **1** was retained after the removal of its lattice water molecules at 140 °C, while compound **2** retained its structure until 200 °C. Further, XRD powder diffractions indicate that the structures of **1** and **2** collapsed and formed amorphous states after the removal of its organic ligands at 400 °C.

The diffuse reflectance UV/Vis spectra of **1** and **2** were investigated with the solid-state sample in $BaSO_4$ pellet (Fig. 10a). The two peaks at about 230 and 335 nm for **1** and **2** are associated with $O_{terminal} \rightarrow V$ and $O_{bridging} \rightarrow V$ charge transfer, respectively. In each case, the broad shoulder centered at 416 nm is assigned to N–Cd and O–Cd charge transfer, whereas the weak wide band around 750 nm is due to *d*–*d* transitions of V^{4+} and Cd^{2+} ions [12]. The band gap energy value was determined by

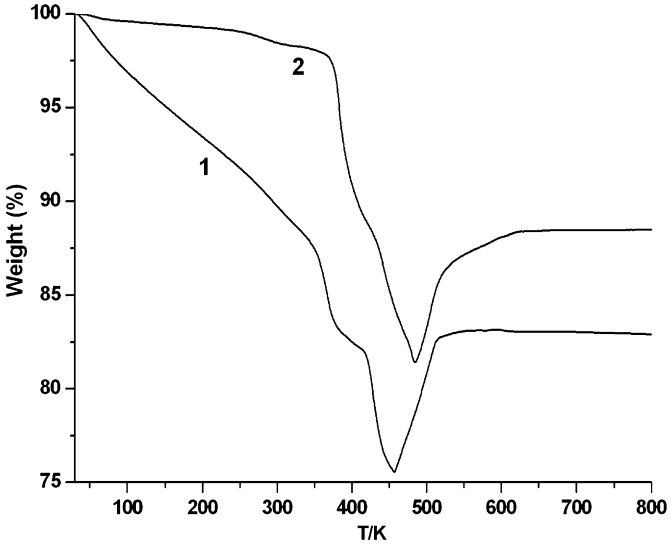

Fig. 7. TGA curves of **1** and **2**.

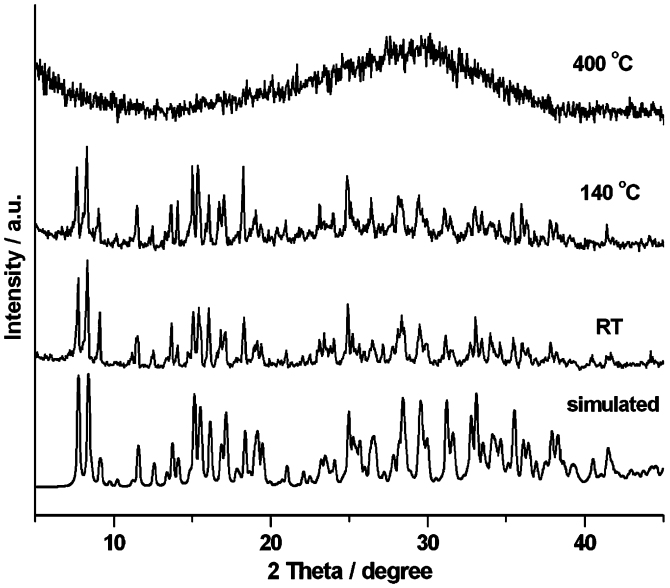

Fig. 9. Powder X-ray diffraction patterns of **2** as simulated from single crystal XRD and variable-temperature XRD patterns.

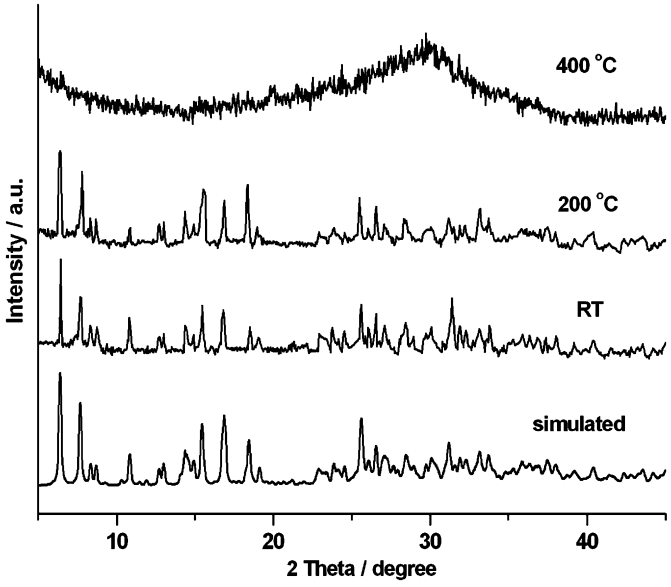

Fig. 8. Powder X-ray diffraction patterns of **1** as simulated from single crystal XRD and variable-temperature XRD patterns.

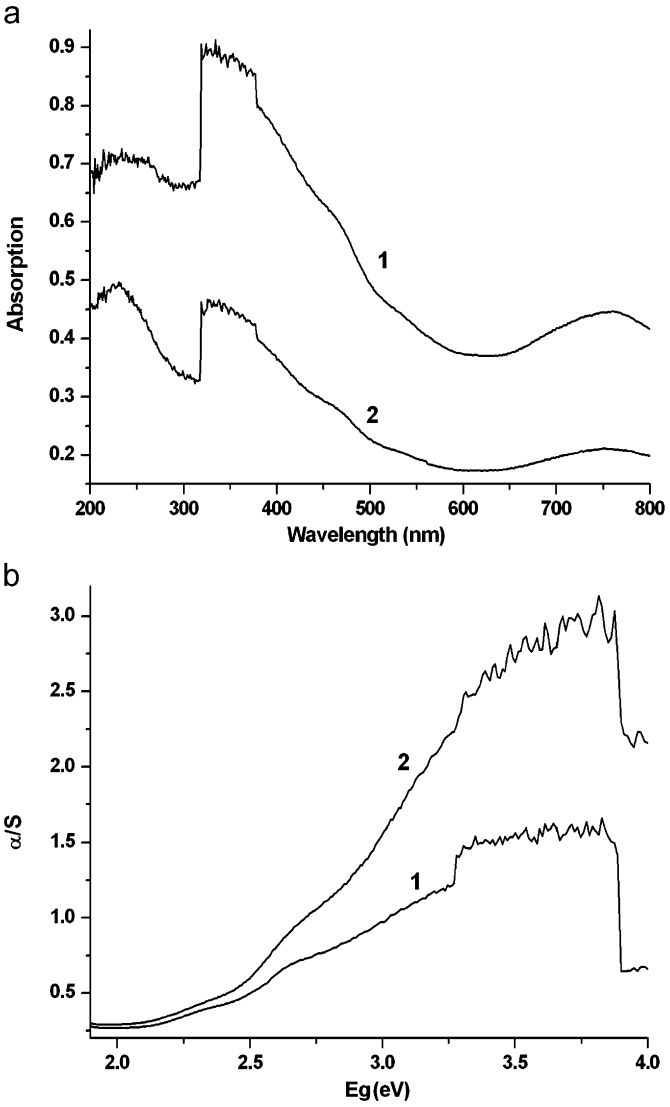

Fig. 10. (a) Optical absorption spectra of **1** and **2** and (b) photon energy dependence of (α/R) for **1** and **2**.

extrapolation from the linear portion of the absorption edge in a (α/S) versus energy plot [13]. The energy band gaps are 2.1 and 2.2 eV for **1** and **2** (Fig. 10b), respectively.

The variable temperature magnetic susceptibility of **1**and **2** were measured between 2 and 300 K. Fig. 11 shows the magnetic behavior of **1** and **2** in the form of $\chi_M T$ vs. temperature, where χ_M is the molar magnetic susceptibility. The magnetism may be attributed solely to the presence of V^{4+} ions ($3d^1, S = 1/2$). The $\chi_M T$ value of the complex **1** at 300 K is 2.49 $cm^3\,K\,mol^{-1}$ (4.46μ_B), much smaller than that expected for the total spin-only value 4.26 $cm^3\,K\,mol^{-1}$ (5.84μ_B) of 12 V^{4+} with $g = 2.0$. The $\chi_M T$ value decreases nearly linearly with decreasing temperature from 2.49 $cm^3\,K\,mol^{-1}$ at 300 K to 0.87 $cm^3\,K\,mol^{-1}$ at 14 K, and then decreases rapidly from 8 K and reaches a minimum value of 0.44 $cm^3\,K\,mol^{-1}$ at 2 K. For **2**, $\chi_M T$ at room temperature is 2.31 $cm^3\,K\,mol^{-1}$ (4.30μ_B), which is also much lower than the value expected for 12 uncoupled electrons (4.26 $cm^3\,K\,mol^{-1}$,

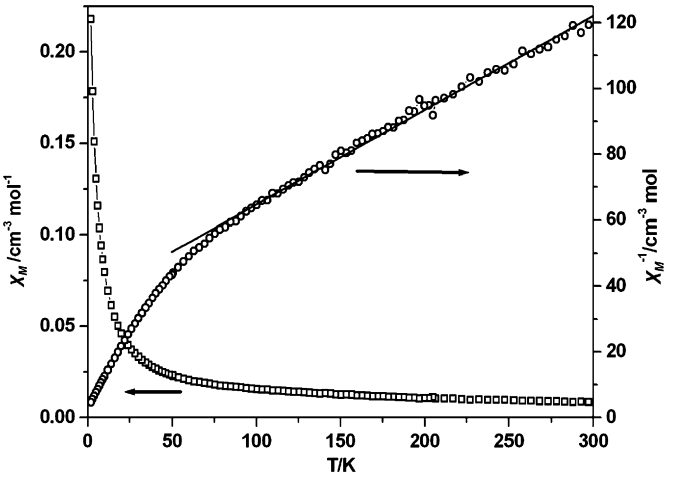

Fig. 12. Temperature dependence of χ_m (□) and χ_m^{-1}(○) for **1**.

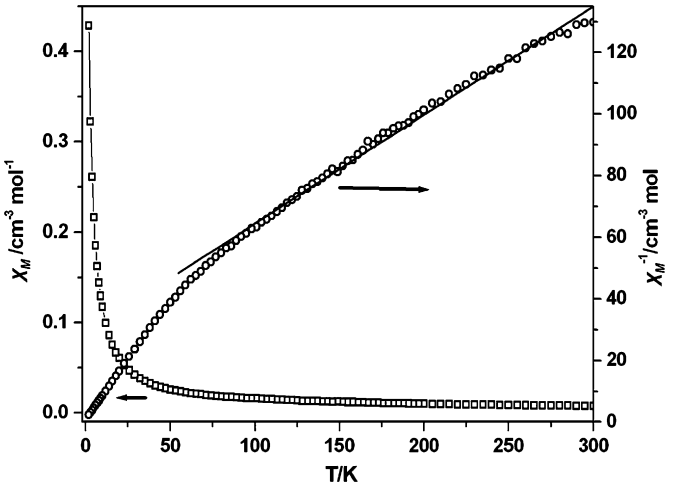

Fig. 13. Temperature dependence of χ_m (□) and χ_m^{-1}(○) for **2**.

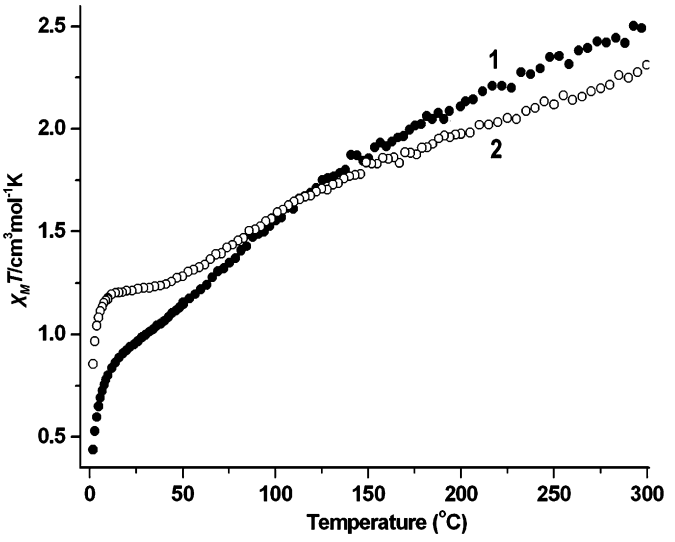

Fig. 11. The temperature dependences of the product $X_M T$ for **1** and **2**.

5.84μ_B, $g = 2.0$). Upon cooling from room temperature, the $\chi_M T$ value decreases nearly linearly until 40 K to stabilize approximately at 1.23 cm^3 K mol^{-1}. Below 12 K, a faster decrease of $\chi_M T$ is observed, with ca.0.86 cm^3 K mol^{-1} at 2 K. The temperature dependences of $\chi_M T$ for **1** and **2** demonstrate the existence of antiferromagnetic coupling interactions between vanadium centers, which is a common feature for most POVs that can be attributed to the electron delocalization on the 12 vanadium sites of each case [14]. The same mechanism might operate in the present systems. In each case, there are 20 connections between the 12 vanadium centers (see Figure S1 in the supporting information), of which 8 involve single μ_3–O bridges (dashed lines) with a V–V average distance of 3.719(2) Å for **1** and 3.719(7) Å for **2**, and the other 12 involve double μ_3–O bridges (solid lines) with a V–V average distance of 2.970(2) Å for **1** and 2.962(6) Å for **2**. These V–V distances have been considered in the literature as acceptable values for charge delocalization among vanadium centers. Both the temperature dependences of the reciprocal susceptibilities ($1/\chi_m$) obey the Curie–Weiss law $\chi = C/(T-\theta)$ in the range of 75–300 K with negative Weiss temperature $\theta = -127.2$ K for **1** and -81.5 K for **2** (Figs. 12 and 13), which support the presence of antiferromagnetic coupling between the V^{4+} ions of both cases. Additionally, the Curie constants $C = 2.83$ cm^3 mol^{-1} K (4.76μ_B) for **1** and 3.49 cm^3 mol^{-1} K (5.28μ_B) for **2** are also lower than the calculated values for 12 uncoupled V^{4+} ions (4.26 cm^3 K mol^{-1}, 5.84μ_B). Unfortunately, it is too difficult to fit the experimental magnetic data of these heteropolymetallic spin system using a suitable theoretical model [15]. Finally, it is notable that a potential role in the occurrences of antiferromagnetic ordering of **1** and **2** may play electron–phonon interactions, which is often observed in those solids whose transition metal–oxygen polyhedra are determined by defect states, including oxygen vacancies and differently substituted metallic cations [16].

In summary, a 0D compound **1** and a 1D compound **2** were successfully synthesized under hydrothermal conditions, which exhibit two rare Cd-substituted POVs. The former is derived from α-{$As_8V_{14}O_{42}$} shell, while the latter is derived from β-{$As_8V_{14}O_{42}$} shell. It is worth noting that **1** is the first di-Cd-substituted POV based on α-{$As_8V_{14}O_{42}$} shell. Further investigation of TM-substituted POVs is in progress.

Acknowledgement

This work was supported by the National Natural Science Fund for Distinguished Young Scholars of China (no. 20725101), the 973 Program (no. 2006CB932904), the NSF of Fujian Province (no. E0510030), the Knowledge Innovation Program of CAS (no. KJCX2.YW.H01), and the NNSF of China (no. 20521101).

Appendix A. Supplementary materials

Supplementary data associated with this article can be found in the online version at doi:10.1016/j.jssc.2008.07.034.

References

[1] (a) J.J. Borrás-Almenar, E. Coronado, A. Müller, M.T. Pope, Polyoxometalate Molecular Science, Kluwer Academic Publishers, Dordrecht, 2004;
(b) J.M. Clemente-Juan, E. Coronado, Coord. Chem. Rev. 361 (1999) 193.
[2] (a) P. Mialane, A. Dolbecq, J. Marrot, E. Rivière, F. Sécheresse, Angew. Chem. Int. Ed. 42 (2003) 3523;
(b) M. Sadakane, M.H. Dickman, M.T. Pope, Angew. Chem. Int. Ed. 39 (2000) 2914;
(c) K. Fukaya, T. Yamase, Angew. Chem. Int. Ed. 42 (2003) 654;

(d) X. Fang, T.M. Anderson, C. Benelli, C. L Hill, Chem. Eur. J. 11 (2005) 712;
(e) R.C. Howell, F.G. Perez, S. Jain, W.D. Horrocks, J.A.L. Rheingold, L.C. Francesconi, Angew. Chem. Int. Ed. 40 (2001) 4031;
(f) U. Kortz, F. Hussain, M. Reicke, Angew. Chem. Int. Ed. 44 (2005) 3773;
(g) J.M. Clemente-Juan, E. Coronado, J.R. Galán-Mascarós, C.J. Gómez-García, Inorg. Chem. 38 (1999) 55;
(h) U. Kortz, I.M. Mbomekalle, B. Keita, L. Nadjo, P. Berthet, Inorg. Chem. 41 (2002) 6412;
(i) I.M. Mbomekalle, B. Keita, M. Nierlich, U. Kortz, P. Berthet, L. Nadjo, Inorg. Chem. 42 (2003) 5143;
(j) Z. Zhang, Y. Li, E. Wang, X. Wang, C. Qin, H. An, Inorg. Chem. 45 (2006) 4313;
(k) S.T. Zheng, D.Q. Yuan, H.P. Jia, J. Zhang, G.Y. Yang, Chem. Commun. 16 (2007) 1858;
(l) S.T. Zheng, J. Zhang, G.Y. Yang, Angew. Chem. Int. Ed. 47 (2008) 3909.
[3] S.T. Zheng, J. Zhang, G.Y. Yang, Eur. J. Inorg. Chem. 10 (2004) 2004.
[4] (a) X.B. Cui, J.Q. Xu, H. Meng, S.T. Zheng, G.Y. Yang, Inorg. Chem. 43 (2004) 8005;
(b) S.T. Zheng, J. Zhang, G.Y. Yang, Inorg. Chem. 44 (2005) 2426;
(c) S.T. Zheng, M.H. Wang, G.Y. Yang, Inorg. Chem. 46 (2007) 9503;
(d) Y.F. Qi, Y.G. Li, C. Qin, E.B. Wang, H. Jin, D.R. Xiao, X.L. Wang, S. Chang, Inorg. Chem. 46 (2007) 3217.
[5] (a) W.W. Wendlandt, H.G. Hecht, Reflectance Spectroscopy, Interscience Publishers, New York, 1966;
(b) G. Kortüm, Reflectance Spectroscopy, Springer, New York, 1969.
[6] G.M. Sheldrick, SADABS, University of Göttingen, Göttingen, Germany, 1997.
[7] G.M. Sheldrick, SHELX TL-97, program for X-ray crystal structure refinement, University of Göttingen, Göttingen, Germany, 1997.
[8] G.H. Huan, M.A. Greaney, A.J. Jacobson, J. Chem. Soc. Chem. Commun. 4 (1991) 260.
[9] S.T. Zheng, J. Zhang, G.Y. Yang, Z. Anorg. Allg. Chem 631 (2005) 170–173.
[10] (a) U. Kortz, S. Nellutla, A.C. Stowe, N.S. Dalal, U. Rauwald, W. Danquah, D. Ravot, Inorg. Chem 43 (2004) 2308;
(b) F. Hussain, L.H. Bi, U. Rauwald, M. Reicke, U. Kortz, Polyhedron 24 (2005) 847–852.
[11] I.D. Brown, D. Altermatt, Acta Crystallogr. B 41 (1985) 244.
[12] M.T. Pope, Heteropoly and Isopoly Oxometalates, Springer, Berlin, 1983.
[13] O. Schevciw, W.B. White, Mater. Res. Bull. 18 (1983) 1059.
[14] (a) A. Müller, F. Peters, M.T. Pope, D. Gatteschi, Chem. Rev. 98 (1998) 239;
(b) A. Müller, R. Sessoli, E. Krickemeyer, H. Bögge, J. Meyer, D. Gatteschi, L. Pardi, J. Westphal, K. Hovemeier, R. Rohlfing, J. Döring, F. Hellweg, C. Beugholt, M. Schmidtmann, Inorg. Chem. 36 (1997) 5239.
[15] O. Kahn, Molecular Magnetism, VCH, Weinheim, Germany, 1993.
[16] I.V. Kityk, M. Makowska-Janusik, J. Appl. Phys 90 (2001) 5542.